Supporting Information

Tungsten Doped Manganese Silicate Films as Stable and Efficient Oxygen Evolution Catalysts in Near-Neutral Media

Shuairu Zhu[1,2], *Jiabo Le*[1], *Jianming Li*[4], *Deyu Liu*[1,3]*, *and Yongbo Kuang*[1,3]*

[1]*Ningbo Institute of Materials Technology and Engineering, Chinese Academy of Sciences, 1219 Zhongguan West Road, Ningbo, Zhejiang 315201, China*

[2]*University of Chinese Academy of Sciences, 19(A) Yuquan Road, Beijing 100049, China*

[3]*Center of Materials Science and Optoelectronics Engineering, University of Chinese Academy of Sciences, 19(A) Yuquan Road, Beijing 100049, China*

[4]*Research Center of New Energy, Research Institute of Petroleum Exploration & Development (RIPED), 20 Xueyuan Road, Beijing 100083, China*

*email: kuangyongbo@nimte.ac.cn (Kuang, Y. B.); liudeyu@nimte.ac.cn (Liu, D. Y.)

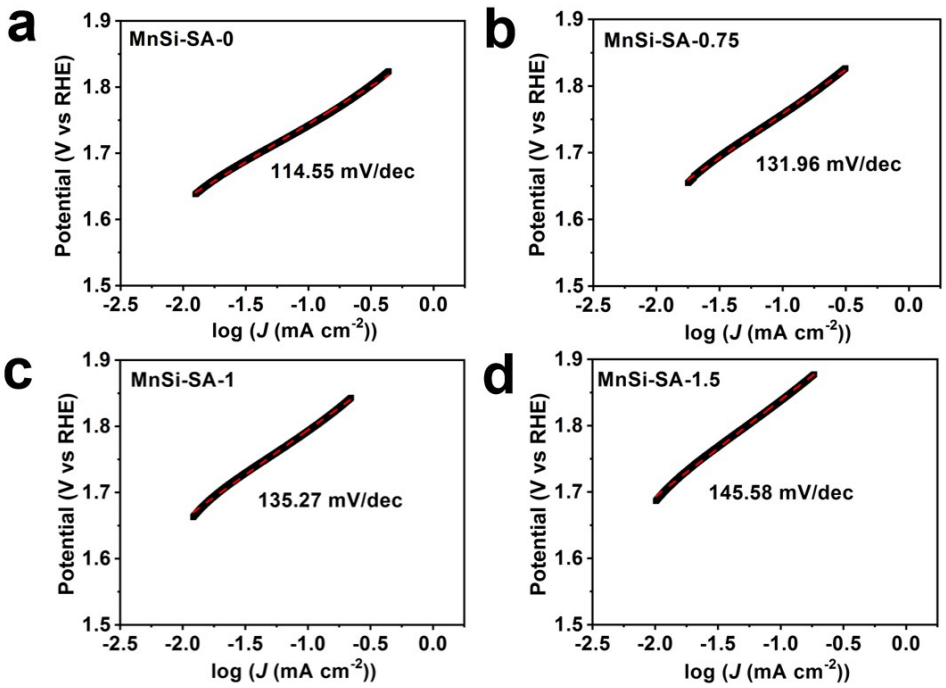

Figure S1. a-d) Tafel plots of the samples in 1 M PBS (pH=7).

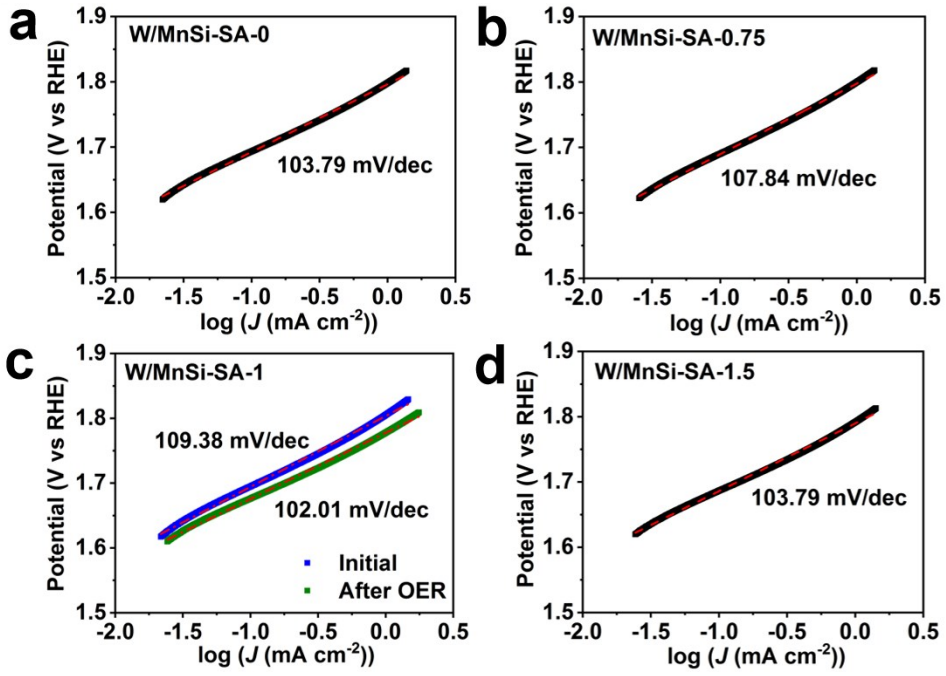

Figure S2. a-d) Tafel plots of the samples in 1 M PBS (pH=7).

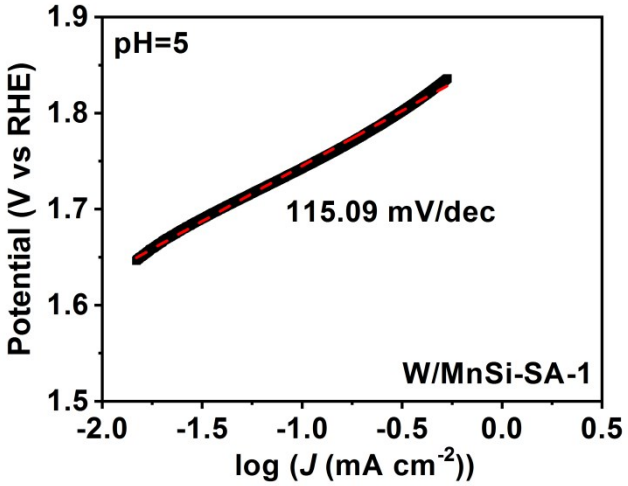

Figure S3. Tafel plot of the W/MnSi-SA-1 in 1 M PBS (pH=5).

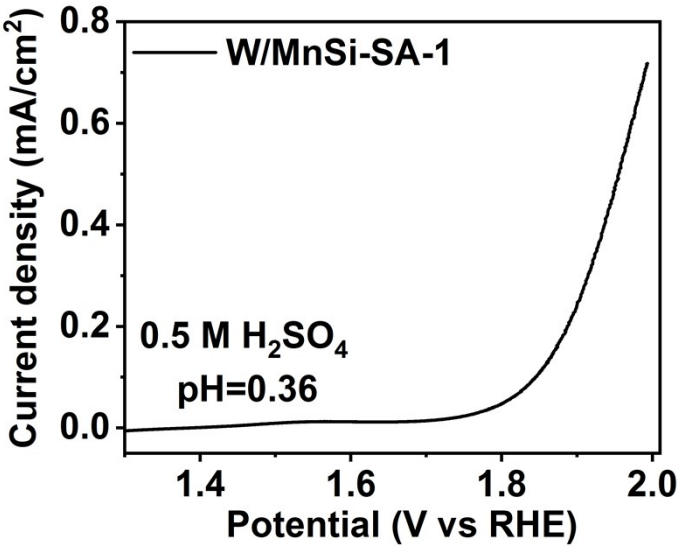

Figure S4. Oxygen evolution properties of the prepared catalysts in acid media (5 mV s^{-1} without *iR* compensation).

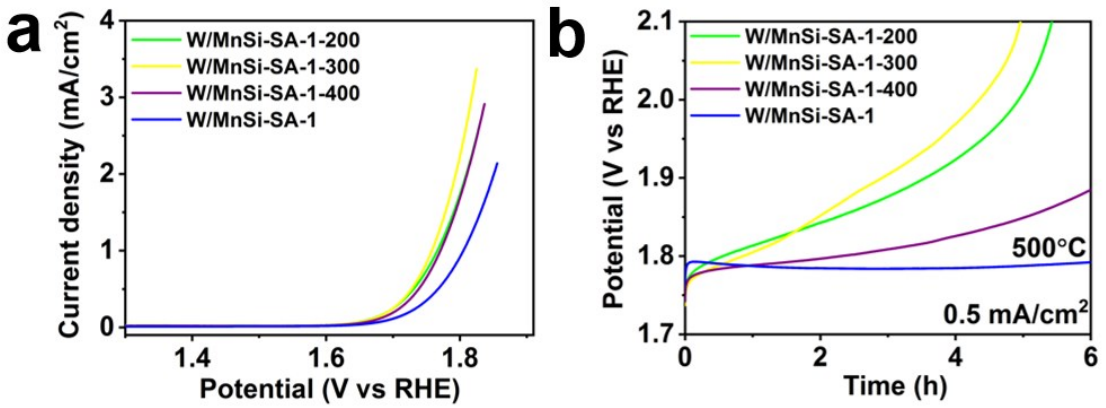

Figure S5. Oxygen evolution properties of the prepared catalysts in 1 M PBS (pH=7). a) polarization curves at a scan rate of 5 mV s^{-1} with *iR* compensation, and b) chronopotentiometric curves for the different calcination temperatures of samples.

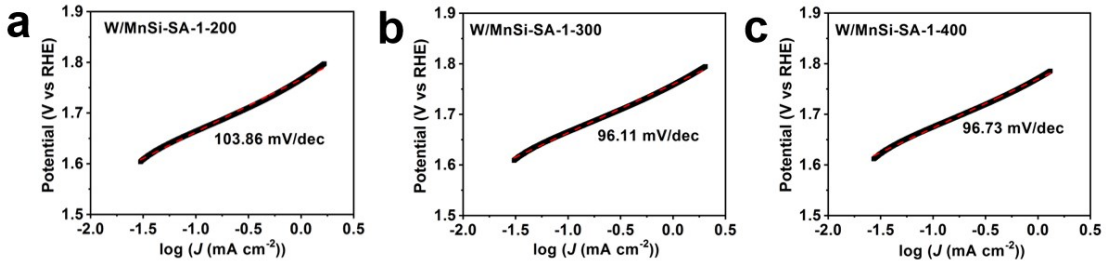

Figure S6. a-c) Tafel plots of the samples in 1 M PBS (pH=7).

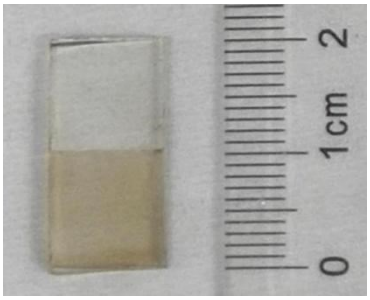

Figure S7. The photograph of W/MnSi-SA-1/FTO.

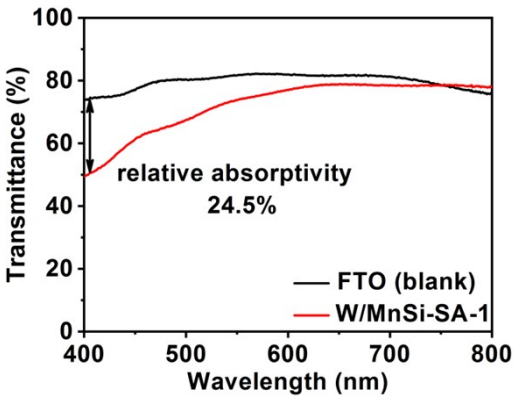

Figure S8. The transparency of W/MnSi-SA-1/FTO.

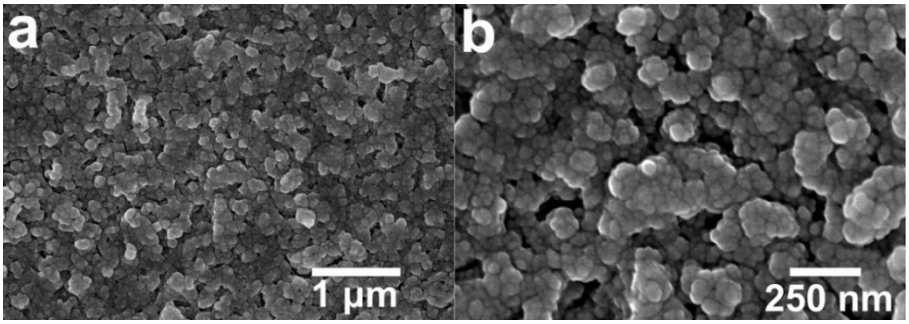

Figure S9. a-b) SEM images of W/MnSi-SA-1 after stability test.

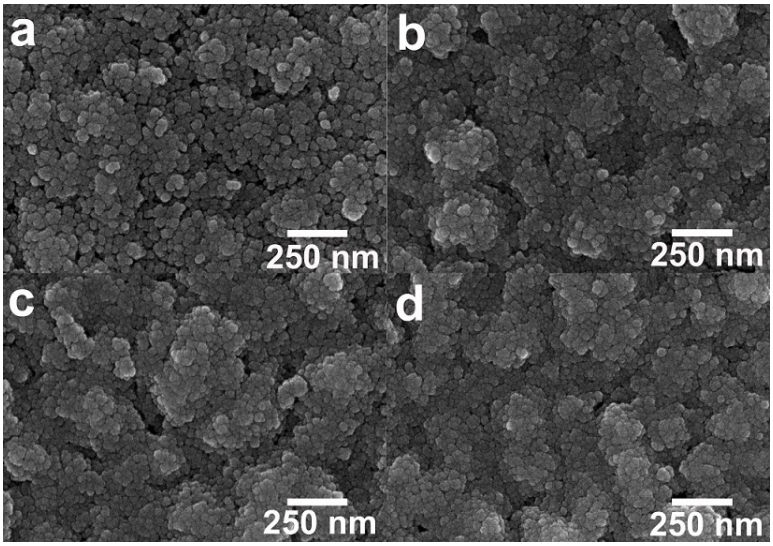

Figure S10. SEM images of a) W/MnSi-SA-1-200, b) W/MnSi-SA-1-300, c) W/MnSi-SA-1-400, d) W/MnSi-SA-1.

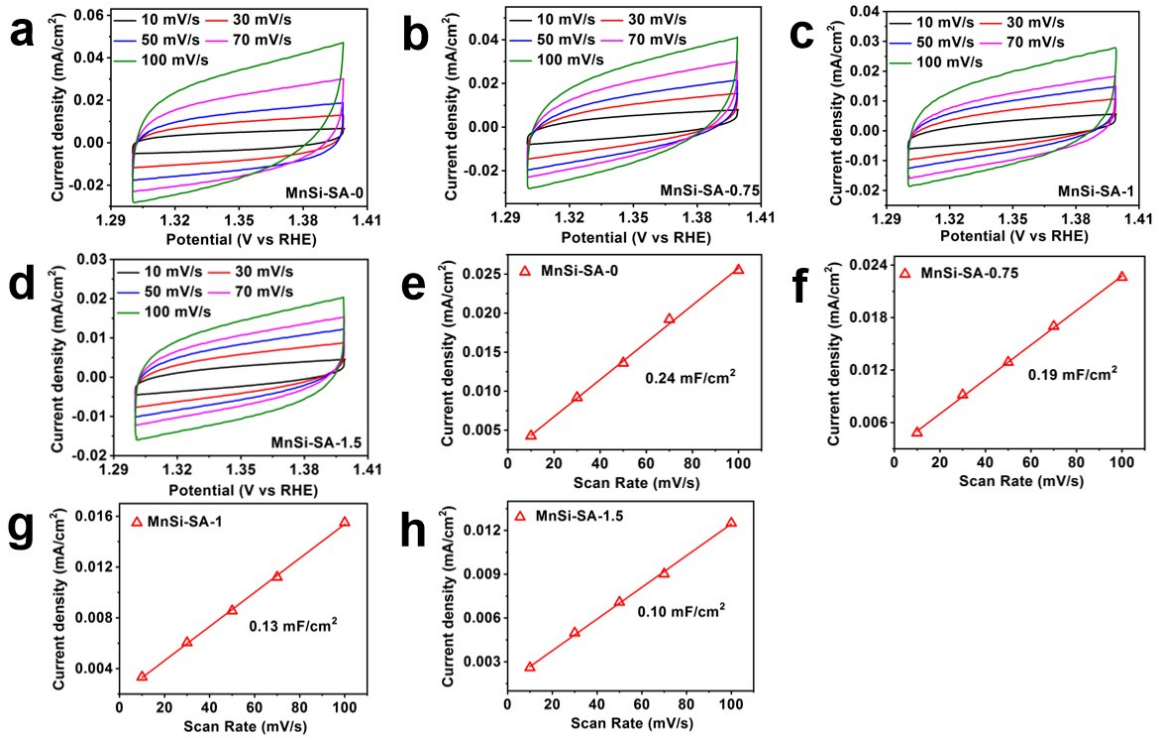

Figure S11. a-d) CV curves of electrodes at scan rate from 10 to 100 mV s^{-1} and e-h) the corresponding evaluation of C_{dl} in 1 M PBS (pH=7).

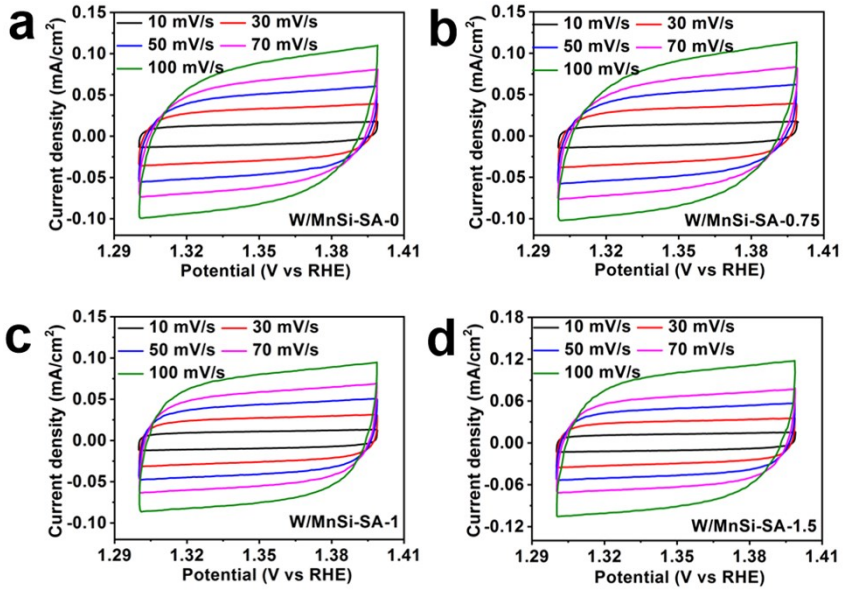

Figure S12. a-d) CV curves of electrodes at scan rate from 10 to 100 mV s^{-1} in 1 M PBS (pH=7).

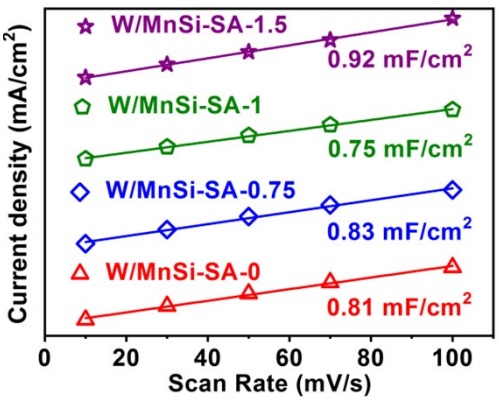

Figure S13. The evaluation of double-layer capacitances (C_{dl}) for the samples in 1 M PBS (pH=7).

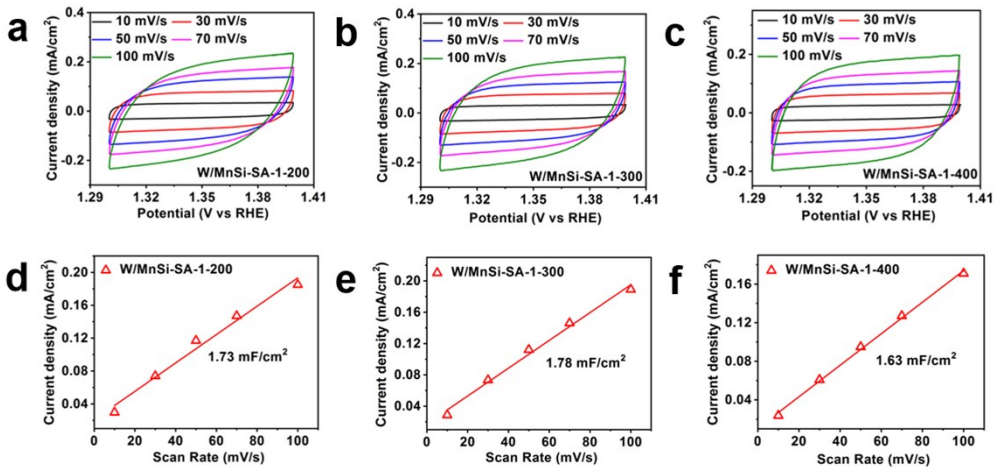

Figure S14. a-c) CV curves of electrodes at scan rate from 10 to 100 mV s^{-1} and d-f) the evaluation of double-layer capacitances (C_{dl}) for the samples in 1 M PBS (pH=7).

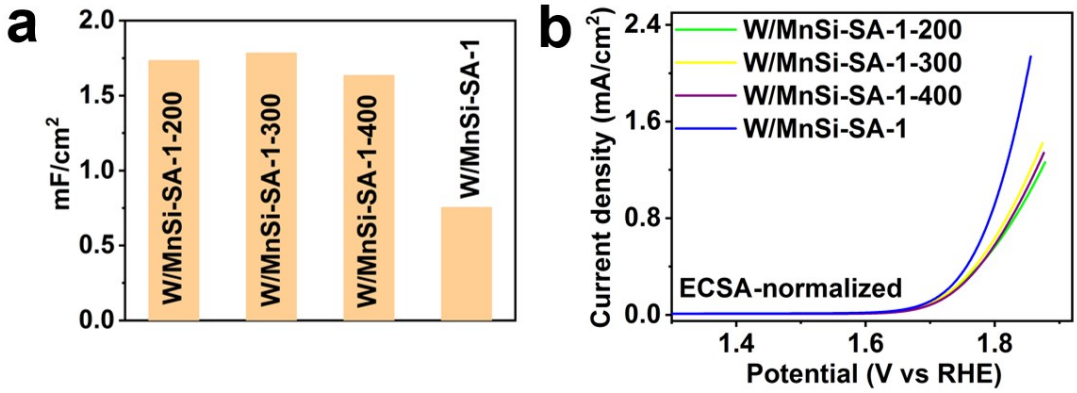

Figure S15. a) the evaluation of double-layer capacitance (C_{dl}) for the samples. b) ECSA normalized OER polarization curves of samples at a scan rate of 5 mV s^{-1} with *iR* compensation in 1 M PBS (pH=7).

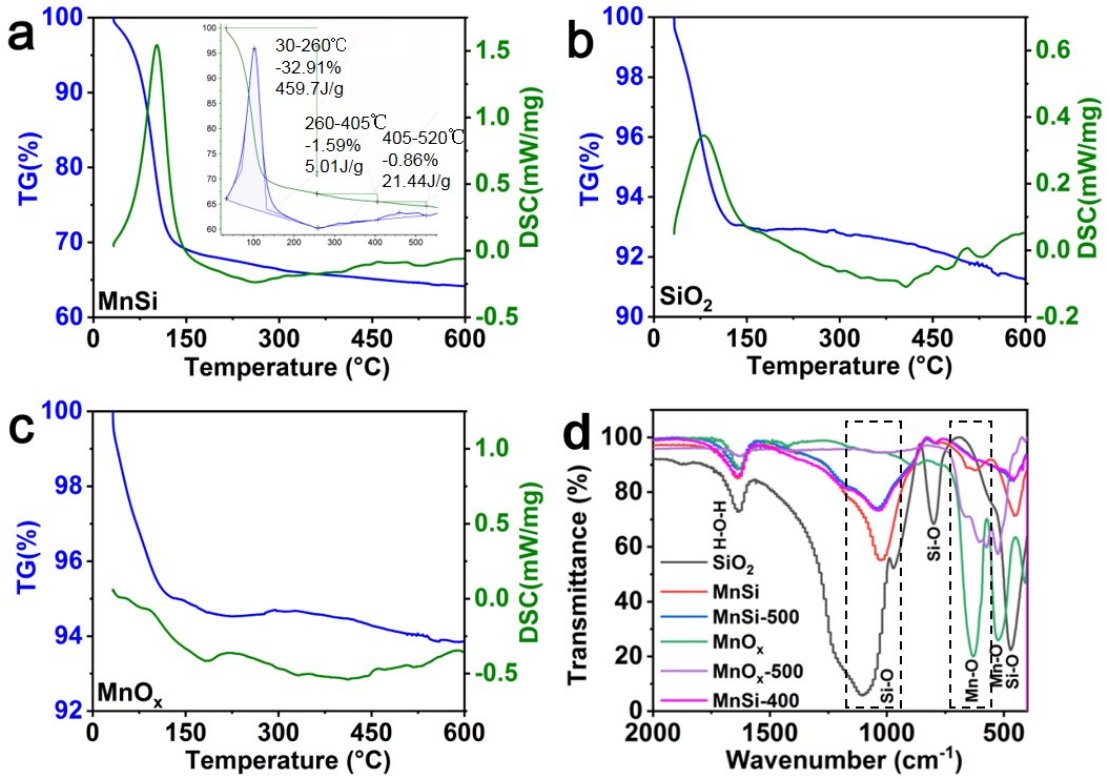

Figure S16. a-c) Thermal analysis of samples under air atmosphere d) FT-IR spectra of samples.

Powders Preparation. The MnSi powder was obtained by microwave reaction. Commercial SiO_2 powder (0.12 g), Manganese acetate ($MnC_4H_6O_4{\cdot}4H_2O$, 2 mmol, Aladdin) and sodium acetate ($NaC_2H_3O_2{\cdot}3H_2O$, 1 mmol, Aladdin) were added into a quartz vial containing a mixed solution of ethanol absolute (10 mL) and deionized water (5 mL) to form a homogeneous solution. Subsequently, the above solution was heated in a microwave reaction apparatus (Explorer 12) to 140 °C for 30 min. After the microwave reaction, the sample was rinsed with deionized water, ethanol and then drying at 60℃. For comparison, MnO_x powder also acquired by same microwave reaction without addition of SiO_2 powder. Finally, MnSi and MnO_x powders are calcinated at 500 ℃ for 2h, named at MnSi-500 and MnO_x-500 respectively. MnSi powder is calcinated at 400 ℃ for 2h, named at MnSi-400.

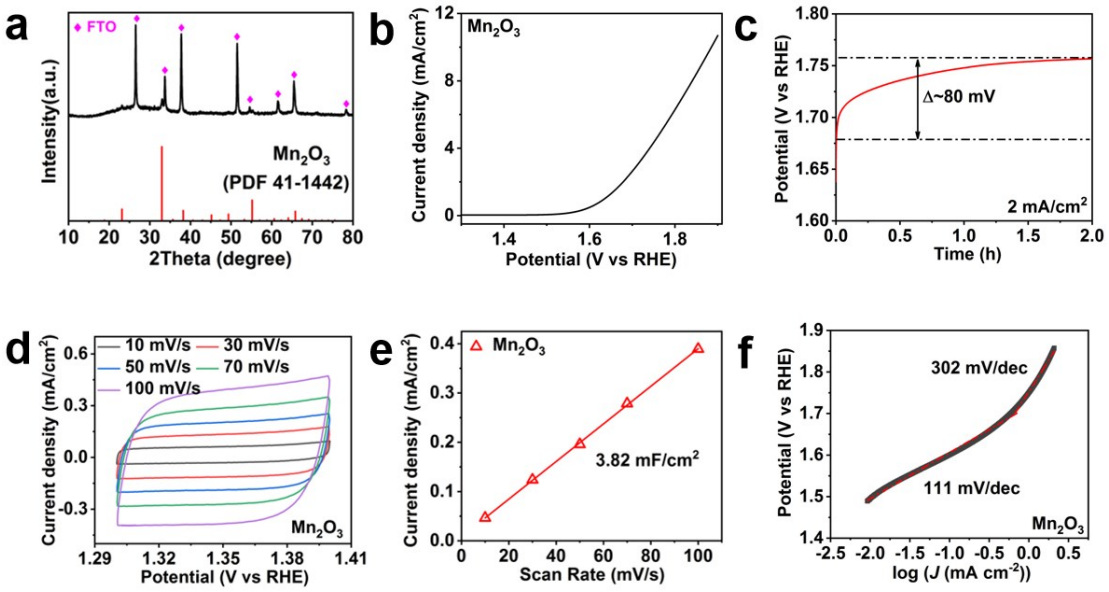

Figure S17. Oxygen evolution properties of the prepared Mn_2O_3 in 1 M PBS (pH=7). (a) XRD patterns. (b) polarization curves of electrode at a scan rate of 5 mV s^{-1} without *iR* compensation. (c) chronopotentiometry curves of electrode with constant current density. (d) CV curves of electrode at scan rate from 10 to 100 mV s^{-1}. (e) the evaluation of double-layer capacitances (C_{dl}). (f) Tafel slopes.

Mn_2O_3 Film Preparation. Mn_2O_3 Film was prepared by galvanostatic deposition onto FTO (1cm×2cm) at a current density of 0.25 mA/cm^2 in a three-electrode system.[1] FTO was used as working electrode. A saturated Ag/AgCl electrode and a platinum wire were used as the reference and counter electrodes, respectively. Electrochemical deposition was carried out in a homogeneous solution of 0.25 M $MnCl_2 \cdot 4H_2O$ and 0.25 M Na_2SO_4 (1:1 ratio) for 10 min. The film was then rinsed thoroughly with deionized water and calcinated at 773 K up to 2 h under air.

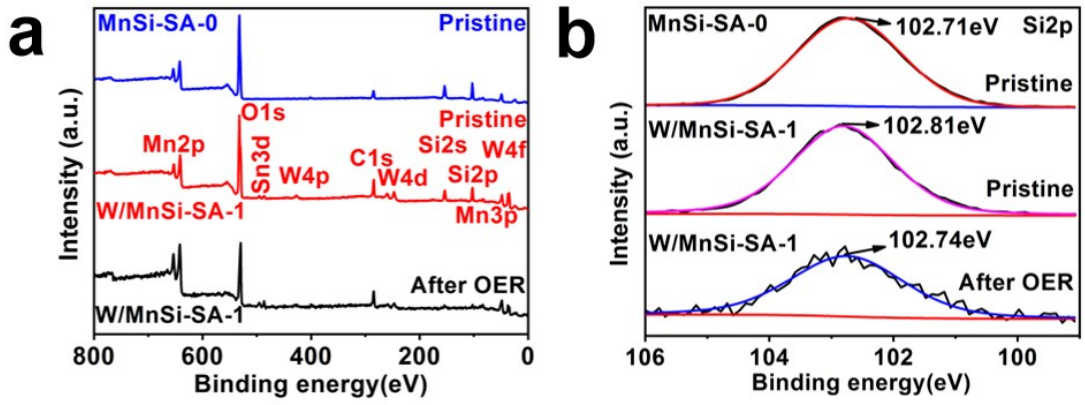

Figure S18. XPS data of the a) survey, and b) Si 2p of the samples.

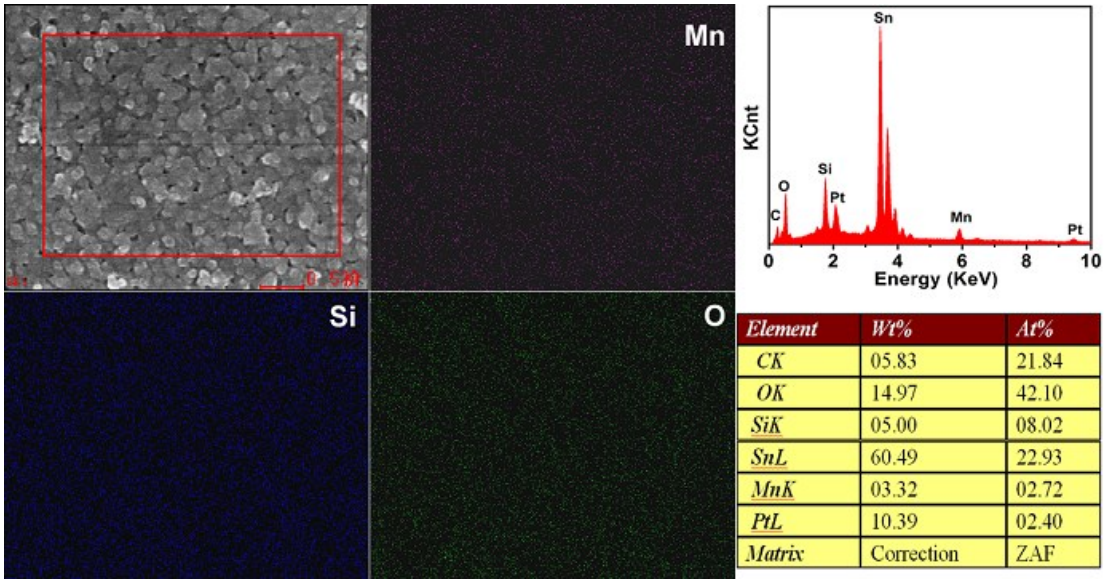

Element	Wt%	At%
CK	05.83	21.84
OK	14.97	42.10
SiK	05.00	08.02
SnL	60.49	22.93
MnK	03.32	02.72
PtL	10.39	02.40
Matrix	Correction	ZAF

Figure S19. The EDS analyses and mapping of W/MnSi-SA-1/FTO.

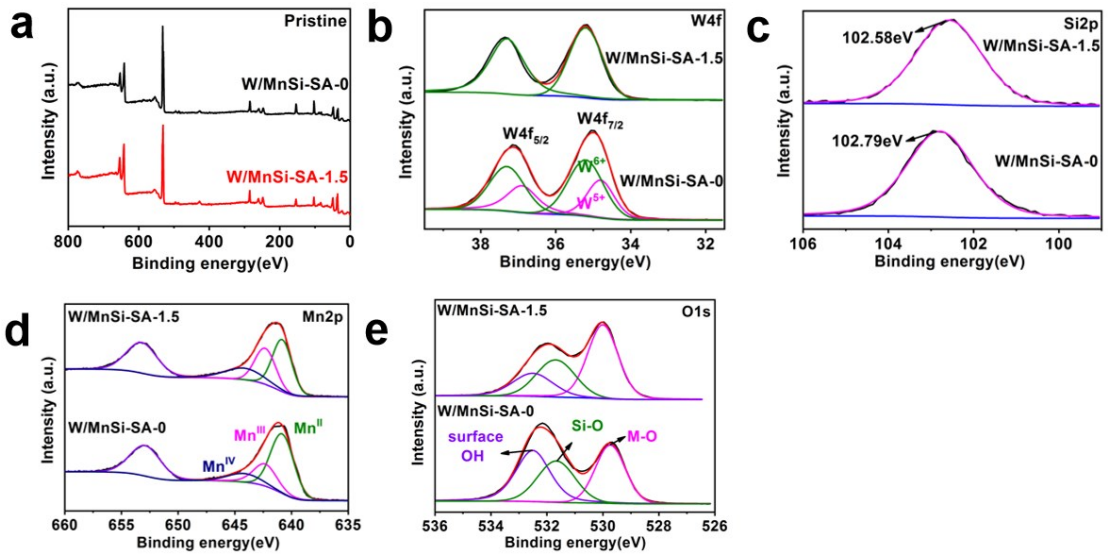

Figure S20. XPS data of the a) survey, b) W 4f, c) Si 2p, d) Mn 2p, and e) O 1s of the samples.

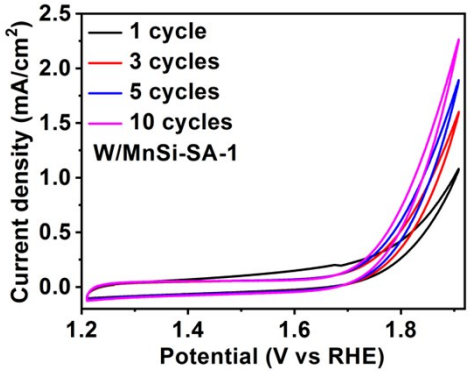

Figure S21. Cyclic voltammetry curves (50 mV s^{-1}) of W/MnSi-SA-1 in 1 M PBS (pH=7).

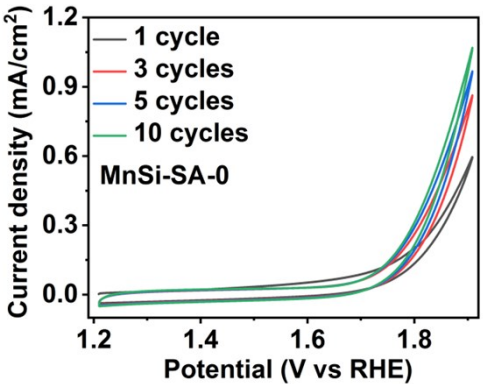

Figure S22. Cyclic voltammetry curves (50 mV s^{-1}) of MnSi-SA-0 1 M PBS (pH=7).

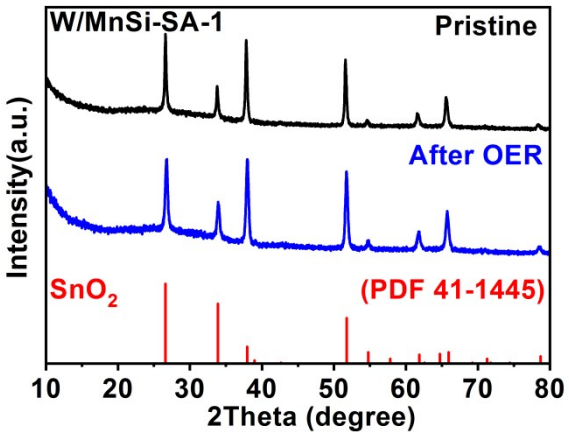

Figure S23. XRD patterns of W/MnSi-SA-1/FTO.

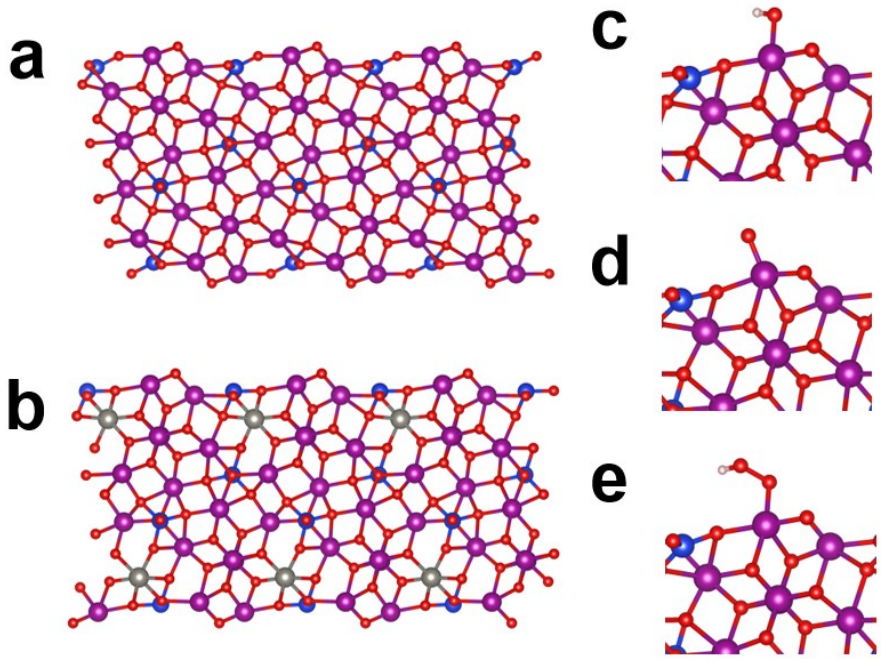

Figure S24. Models of $Mn_4SiO_7(100)$ surface (a) and $W_xMn_{4-x}SiO_7(100)$ surface (b). (c)-(e), $Mn_4SiO_7(100)$ surfaces with adsorbed OH*, O* and OOH*, respectively. The purple, grey, blue, red and white balls represent Mn, W, Si, O and H atoms, respectively.

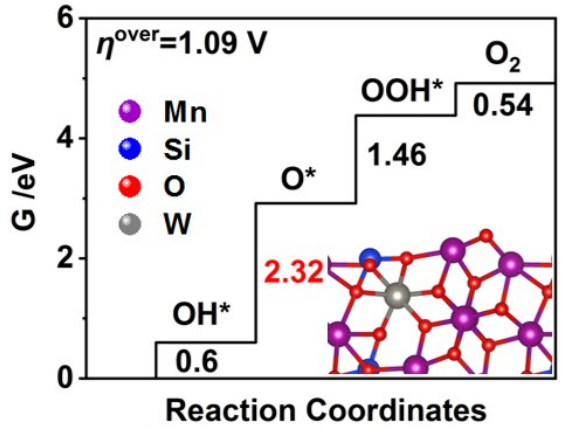

Figure S25. Gibbs free-energy diagram for $W_xMn_{4-x}SiO_7$ (The inset shows the $W_xMn_{4-x}SiO_7(100)$ surface).

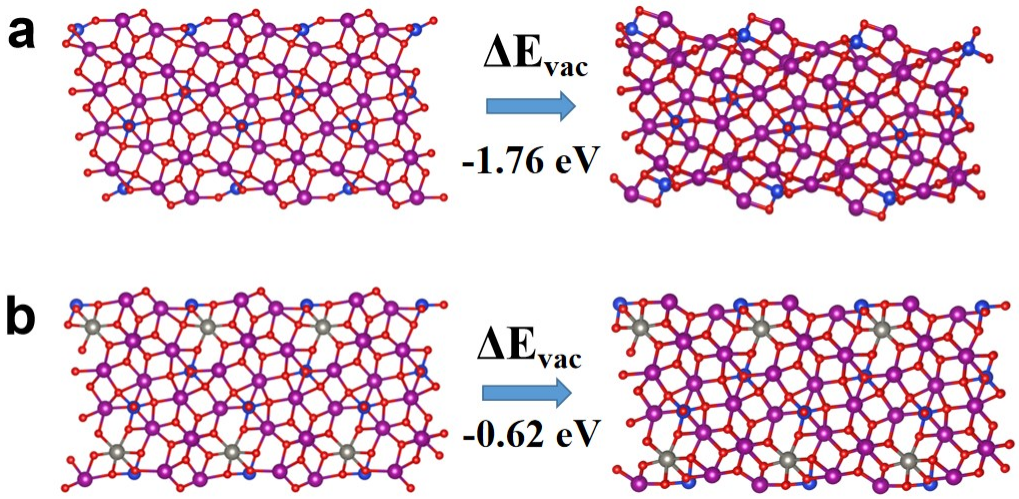

Figure S26. The calculated formation energies of oxygen vacancies on a) $Mn_4SiO_7(100)$, and b) $W_xMn_{4-x}SiO_7(100)$ surfaces. It is shown that the structure of the $Mn_4SiO_7(100)$ surface has significant reconstruction after the formation of oxygen vacancy. In contrast, the doping of W greatly reduces this deformation, suggesting that the doping of W has a significant promoting effect on the stability of the structure.

Table S1. Naming rules.

samples	method		
	evaporator source	sodium acetate	calcination temperature
MnSi-SA-0	SiO_2	0 mmol	773 K
MnSi-SA-0.75	SiO_2	0.75 mmol	773 K
MnSi-SA-1	SiO_2	1 mmol	773 K
MnSi-SA-1.5	SiO_2	1.5 mmol	773 K
W/MnSi-SA-0	SiO_2+W	0 mmol	773 K
W/MnSi-SA-0.75	SiO_2+W	0.75 mmol	773 K
W/MnSi-SA-1	SiO_2+W	1 mmol	773 K
W/MnSi-SA-1.5	SiO_2+W	1.5 mmol	773 K
W/MnSi-SA-1-200	SiO_2+W	1 mmol	473 K
W/MnSi-SA-1-300	SiO_2+W	1 mmol	573 K
W/MnSi-SA-1-400	SiO_2+W	1 mmol	673 K

Table S2. The comparison of the electrochemical preformances of Mn-based and noble metal oxygen evolution catalysts in near-neutral media.

catalysts	pH/electrolyze	Tafel slop [mV dec^{-1}]	overpotential [mV vs RHE]	durability	Ref.
W/MnSi-SA-1	pH=7 1M PBS	109.38	538	0.5 mA cm^{-2} for 6 h (nearly no increase of overpotential)	this work
W/MnSi-SA-1	pH=5 1M PBS	115.09	603	0.3 mA $cm^{-2}$for 15 h (slightly increase of overpotential about 13.5 mV)	this work
Mn_2O_3	pH=7 1M PBS	111	450	2 mA cm^{-2} (0.39 mA cm^{-2} by ECSA normalized) for 2 h (rapidly increase of overpotential about 80 mV)	this work
MnO_x-573K α-Mn_2O_3 Mn_3O_4	neutral 1M KPi	–	470	all samples displayed a fast degradation for current density during 1 h	1
α-MnO_2 β-MnO_2 γ-MnO_2 δ-MnO_2 λ-MnO_2 R-MnO_2 Mn_3O_4 Mn_2O_3 $LiMn_2O_4$	0.1 M NaPi pH =7	–	585	these oxides showed the activities of a significant decrease during 30 min except γ-MnO_2	2
Mn_5O_8 nanoparticles	pH=7.8 0.3 M PBS	78.7	580	5 mA cm^{-2} for 5000s	3
$Mn_3(PO_4)_2 \cdot 3H_2O$	0.5 M NaPi pH =7	120	680 (0.316 mA cm^{-2})	1.813 V vs RHE for 2 h	4
$LiMnP_2O_7$	0.5 M NaPi pH =7	120	680 (0.5 mA cm^{-2})	1.813 V vs RHE for 2 h	5
activated MnO_x	0.1 M PBS pH =7	~70	470	0.1 mA/cm^2 for 8 h	6
RuO_2	0.1 M PBS pH =7	200	395 (2 mA cm^{-2})	–	7
IrO_2	1 M PBS pH =7	132.1	431 (10 mA cm^{-2})	–	8
RuO_2	1 M PBS pH =7	157	~590 (10 mA cm^{-2}) ~370 (3 mA cm^{-2})	10 mA cm^{-2} for 5.5 h (increase of overpotential about 100 mV)	9
IrO_2	neutral 1 M PBS	164.7	343 (10 mA cm^{-2})	current density was decreased by 85 % in 10 h for Pt/C-IrO_2	10

Table S3. Atomic percentage (AP) of samples by XPS.

samples	AP

	Si	Mn	W	O
MnSi-SA-0	23.75	9.51	0	66.73
W/MnSi-SA-0	18.28	12.35	1.59	67.77
W/MnSi-SA-1.5	13.09	16.82	2.61	67.47
W/MnSi-SA-1	8.12	22.82	1.81	67.24
(After OER)				
W/MnSi-SA-1	19.77	10.16	2.11	67.95

Table S4. Binding energy (BE) and relative peak area (PA) of O 1s, and molar percentages (MP) of M-O, Si-O and OH species of samples.

Sample name	BE(eV)			PA(Counts)			MP(%)
	M-O	Si-O	OH	M-O	Si-O	OH	OH
MnSi-SA-0	529.95	531.68	532.5	69840.01	92539.84	150170.4	48
W/MnSi-SA-0	529.74	531.66	532.5	109151.6	123928.1	96089.26	29.2
W/MnSi-SA-1.5	530.00	531.68	532.5	148137.5	88341.35	61469.15	20.6
W/MnSi-SA-1	529.85	531.37	525.52	28778.05	9325.445	12665.65	24.9
(After OER)							
W/MnSi-SA-1	529.71	531.53	532.5	76778.95	56755.41	129701.4	49.3

Table. S5. Binding energy (BE) and relative peak area (PA) of W 4f, molar percentages (MP) of W^{5+} and W^{6+} species, and average valence state (AVS) of samples.

Sample name	BE(eV)				PA(Counts)				MP(%)		AVS
	W^{5+}	W^{5+}	W^{6+}	W^{6+}	W^{5+}	W^{5+}	W^{6+}	W^{6+}	W^{5+}	W^{6+}	
	$4f_{5/2}$	$4f_{7/2}$	$4f_{5/2}$	$4f_{7/2}$	$4f_{5/2}$	$4f_{7/2}$	$4f_{5/2}$	$4f_{7/2}$			
MnSi-SA-0	—	—	—	—	—	—	—	—	—	—	—
W/MnSi-SA-0	36.9	34.8	37.3	35.2	6770.818	7452.779	10576.14	13112.23	37.52	62.48	5.62
W/MnSi-SA-1.5	—	—	37.3	35.2	—	—	28839.6	28157.96	—	100	6
W/MnSi-SA-1	36.9	34.8	37.3	35.2	1242.387	1677.89	2114.248	2659.991	37.95	62.05	5.62
(After OER)											
W/MnSi-SA-1	36.9	34.8	37.3	35.2	13229.69	18377.74	5762.298	6985.271	71.26	28.74	5.29

Table. S6. Binding energy (BE) and relative peak area (PA) of Mn 2p, molar percentages (MP) of Mn^{2+}, Mn^{3+} and Mn^{4+} species, and average valence state (AVS)

of samples.

Sample name	BE(eV)			PA(Counts)			MP(%)			AVS
	Mn^{2+}	Mn^{3+}	Mn^{4+}	Mn^{2+}	Mn^{3+}	Mn^{4+}	Mn^{2+}	Mn^{3+}	Mn^{4+}	
	$2p_{3/2}$	$2p_{3/2}$	$2p_{3/2}$	$2p_{3/2}$	$2p_{3/2}$	$2p_{3/2}$				
MnSi-SA-0	640.82	642.31	644.17	48702.71	45085.5	25647.11	40.8	37.7	21.5	2.807
W/MnSi-SA-0	640.82	642.32	644.17	98980.09	41044.57	21611.15	61.2	25.4	13.4	2.522
W/MnSi-SA-1.5	640.82	642.32	644.17	93398.95	67855.68	45870.73	45.1	32.8	22.1	2.773
W/MnSi-SA-1	640.82	642.31	644.18	14520.45	16910.17	11995.6	33.4	38.9	27.7	2.943
(After OER)										
W/MnSi-SA-1	640.81	642.30	644.13	71559.58	19375.81	15093.69	67.5	18.3	14.2	2.467

Notes and references

1 A. Ramírez, P. Hillebrand, D. Stellmach, M. M. May, P. Bogdanoff and S. Fiechter, Evaluation of MnO_x, Mn_2O_3, and Mn_3O_4 electrodeposited films for the oxygen evolution reaction of water, *J. Phys. Chem. C*, 2014, **118**, 14073-14081.

2 R. Pokhrel, M. K. Goetz, S. E. Shaner, X. X. Wu and S. S. Stahl, The "Best Catalyst" for water oxidation depends on the oxidation method employed: a case study of manganese oxides, *J. Am. Chem. Soc.*, 2015, **137**, 8384-8387.

3 D. Jeong, K. Jin, S. E. Jerng, H. M. Seo, D. H. Kim, S. H. Nahm, S. H. Kim and K. T. Nam, Mn_5O_8 nanoparticles as efficient water oxidation catalysts at neutral pH, *ACS Catal.*, 2015, **5**, 4624-4628.

4 K. Jin, J. Park, J. Lee, K. D. Yang, G. K. Pradhan, U. Sim, D. Jeong, H. L. Jang, S. Park, D. Kim, N. E. Sung, S. H. Kim, S. Han and K. T. Nam, Hydrated manganese(II) phosphate ($Mn_3(PO_4)_2 \cdot 3H_2O$) as a water oxidation catalyst, *J. Am. Chem. Soc.*, 2014, **136**, 7435-7443.

5 J. Park, H. Kim, K. Jin, B. J. Lee, Y.-S. Park, H. Kim, I. Park, K. D. Yang, H.-Y. Jeong and J. Kim, A new water oxidation catalyst: lithium manganese pyrophosphate with tunable Mn valency, *J. Am. Chem. Soc.*, 2014, **136**, 4201-4211.

6 M. Huynh, C. Y. Shi, S. J. L. Billinge and D. G. Nocera, Nature of activated manganese oxide for oxygen evolution, *J. Am. Chem. Soc.*, 2015, **137**, 14887-14904.

7 Y. T. Xu, Z. M. Ye, J. W. Ye, L. M. Cao, R. K. Huang, J. X. Wu, D. D. Zhou, X. F. Zhang, C. T. He, J. P. Zhang and X. M. Chen, Non-3d metal modulation of a cobalt imidazolate framework for excellent electrocatalytic oxygen evolution in neutral media, *Angew. Chem. Int. Ed.*, 2019, **58**, 139-143.

8 Y. K. Zhang, C. Q. Wu, H. L. Jiang, Y. X. Lin, H. J. Liu, Q. He, S. M. Chen, T. Duan and L. Song, Atomic iridium incorporated in cobalt hydroxide for efficient oxygen evolution catalysis in neutral electrolyte, *Adv. Mater.*, 2018, **30**, 1707522.

9 B. B. Jiang, X. Fan, Q. Dang, F. Liao, Y. Y. Li, H. P. Lin, Z. H. Kang and M. W. Shao, Functionalization of metal oxides with thiocyanate groups: A general strategy for boosting oxygen evolution reaction in neutral media, *Nano Energy*, 2020, **76**, 105079.

10 F. Luo, L. Guo, Y. H. Xie, J. X. Xu, K. G. Qu, Z. H. Yang, Iridium nanorods as a robust and stable bifunctional electrocatalyst for pH universal water splitting, *Appl. Catal. B-Environ.*, 2020, **279**, 119394.